Search for Low Energy Structures of Water Clusters $(H_2O)_n$, $n = 20-22$, 48, 123, and 293

Jan K. Kazimirski† and Victoria Buch*

The Fritz Haber Institute for Molecular Dynamics, Hebrew University, Jerusalem 91904, Israel

Received: April 30, 2003; In Final Form: September 2, 2003

A search for low energy structures of water clusters was performed with a combination of three computational tools: (a) temperature-dependent classical trajectories; (b) hydrogen network improvement; (c) rigid body diffusion Monte Carlo calculation on a smoothed potential energy surface. For the sizes of our main interest, $n = 48$, 123, and 293, input configurations included spheroid structures cut from crystalline ice, and amorphous structures. For $n = 48$, tube and sandwich minima were explored as well. The lowest energy configurations found were characterized by compact three-dimensional shapes. In the case of $n = 48$ and 123, crystallinity was lost in the course of the optimization; for these sizes, one finds four-, five-, and six-membered rings of water molecules, On the other hand, the lowest energy structure found for $n = 293$ includes a crystal core, dominated by six-membered rings, and an amorphous surface.

I. Introduction

During the last years, study of gaseous water clusters became an important branch of H_2O research for the following reasons: (a) detailed spectroscopic data became available for $(H_2O)_n$ in a broad size range; (b) a combination of theoretical and experimental investigations on water clusters are a valuable source of information on interactions between water molecules (this information can be further used for study of "real life" condensed phases); (c) clusters can be considered a bridge between the gas phase and the condensed phases, and therefore, evolution toward condensed phase structure and dynamics as a function of size is of interest; (d) H_2O particles and perhaps also clusters play an important role in atmospheric and space chemistry, and cluster studies may contribute to the understanding of the pertinent processes;[1] (e) $(H_2O)_n$ clusters display a variety of interesting behaviors and are therefore worthy of basic research for their own sake. The present study focuses on low energy structures of $(H_2O)_n$ in the size range which is not yet well understood, of tens to hundreds of molecules. Specifically, the representative sizes $n = 48$, 123, and 293 were investigated. Calculations were also carried out for $n = 20-22$, mostly for calibration purposes and for comparison.

A. Past Studies. For the water dimer, a sequence of past experimental and theoretical studies (see, e.g., refs 2 and 3) demonstrated conclusively a near-linear hydrogen bonded global minimum on the potential energy surface (PES). $(H_2O)_n$, $n \geq 3$, clusters have been investigated extensively for a long time, in theoretical studies employing electronic structure techniques (e.g., refs 4−22), a variety of analytical potentials (e.g., refs 23−48), and a combination of both (e.g., refs 49−57). For $n = 3-5$, a cyclic lowest energy structure has been predicted, with the basic structural unit of a single proton donor−single acceptor water molecule. A transition to three-dimensional structures was obtained near $n = 6$ (e.g., refs 9, 49, 50, and 56). For the octamer, two very stable cubic structures (S_4 and D_{2d}) were predicted.[29,49,52] A series of far-infrared vibration−rotation−tunneling[58] and infrared laser spectroscopic studies[59] confirmed a cyclic structure for $n = 3-5$ and demonstrated a transition to a three-dimensional cage structure at $n = 6$.[60] Similar conclusions were drawn from the double resonance ion-dip infrared experiments on water clusters connected to benzene[9,61] and to phenol.[62,63] The stable symmetric cube structures of the octamer were reported for the $(H_2O)_8$−benzene cluster[64] and for water clusters with the phenol chromophore.[65] Measurement of size selected infrared spectra of $(H_2O)_n$ in the $n = 7-10$ range, in conjunction with calculations, resulted in assignment to single cage structures. The $n = 7-10$ minimum energy structures can be viewed as derived from the octamer cube, by addition or subtraction of molecules.[66−68]

For the $n = 11-30$ size range, considerable insight has been gained from theoretical studies (see, e.g., refs 13, 22, 27, 31, 36, 38, 39, 43, 44, 46, 47, 53, and 54). The global minima in this range can be viewed as "multiple fused cage" structures. Most recently, structural evolution as a function of size in this range was addressed systematically by Hartke,[47] for the TIP4P[69] and TTM2-F[70] potentials. Clusters at the low end of this size range have been described by him as "all surface". Increase in size is marked by appearance of three-dimensional "centered cage" forms with one or two four-coordinated core molecules in the interior. A number of theoretical studies focused on simulations of the melting transition in water clusters (e.g., refs 23, 24, and 45), and on investigations of "special" structures which were proposed to be particularly interesting and/or stable. The proposed special forms included clusters composed of cubic octamer-like subunits,[28,29] tubes of five- and six-membered water rings,[48] flat sandwich-like structures,[42] and large spheroid single cages.[15,39]

Starting from sizes of "several tens of molecules", *investigation of the evolution of general structural characteristics as a function of mean size* appears more meaningful than a search for a single ground state for consecutive cluster sizes, for any potential. This is since very numerous low energy structures of similar energies are expected for each size. Determination of the exact energy ordering of these structures would require potentials of presently unavailable accuracy. Moreover, most of the available experimental data for neutral $(H_2O)_n$ clusters pertain to *distributions* of cluster sizes rather than to a single

* To whom correspondence should be addressed. E-mail: viki@fh.huji.ac.il.
† E-mail: jankazim@fh.huji.ac.il.

10.1021/jp0305436 CCC: $25.00
Published on Web 00/00/0000 PAGE EST: 13.3

known size,[71−76] although there are interesting current advances in spectroscopy of size-selected water clusters doped with an Na atom.[75]

The investigation of clusters in the next "nanoparticle" range (hundreds to thousands of molecules) corresponds to the onset of crystallinity. The crystalline ice structure is favorable for the ice interior rather than for the icy surface and, therefore, appears for particle sizes with a sufficient amount of the four-coordinated interior. The published electron diffraction studies revealed crystalline diffraction patterns characteristic of cubic ice in the range of thousands of H_2O molecules,[71,72] starting from $n \sim 1000$; the data indicated, however, the presence of a concurrent disordered component. Clusters containing ∼200 molecules were proposed to be amorphous, based on their diffraction patterns.[71]

Consistent experimental evidence emerged in a recent spectroscopic study of the Devlin group,[73,74] in measurements of bond stretch spectra as a function of mean cluster size. It was shown that the OH and OD stretch spectra of clusters in the size range 1000−100000 can be decomposed to three components, which were assigned, respectively, to particle surface, subsurface, and crystalline interior. These data were interpreted using our preliminary simulations, for a cluster with 979 molecules. The cluster was "cut out" from a cubic ice crystal structure and subjected to surface relaxation by a short classical trajectory, followed by minimization. The following physical picture emerged. Minimization of the surface area of a particle requires a geometry which is close to spherical. However, a spherical crystal surface would include numerous dangling H and O atoms, with unsatisfied H-bond coordination. Therefore, the surface reconstructs so as to increase the number of hydrogen bonds, while "recombining" many of the dangling atoms; the reconstruction occurs at the expense of crystalline order. Many of these surface bonds are highly strained. The subsurface corresponds to a transition region between the surface and the crystalline interior; the locations of the O atoms in the subsurface are close to the crystal sites; however, some strain and distortion occurs in the hydrogen bond network, due to the interaction with the surface. A perfect crystalline interior component, matching bulk ice spectra, was identified spectroscopically starting from a mean diameter of 4 nm ($n \approx 1000$). Smaller nanoparticles of several hundred molecules were still proposed to include a crystal core, albeit stretched by the interaction with the disordered surface, as evidenced by the persistence of the spectroscopic "subsurface" signature down to these sizes, together with the "surface" signature similar to that of the larger sizes. At $n \sim 100$ the spectrum no longer appears as a superposition of these two components but rather resembles that of amorphous ice. *These results suggest onset of a (strained) crystal core at a size of a few hundred molecules.* Recently, measurements of FTIR spectra as a function of mean cluster size were extended by Bauerecker et al. down to sizes of tens of water molecules.[76] Buck et al. studied the tens to hundreds size range using mass spectrometric detection of fragments. Comparison of the measured spectra with the spectra calculated with the cluster models generated in this study will be presented in a sepatate publication.[77]

B. Search for Low Energy Structures of Water Clusters: Introduction. *Structural Characteristics.* Water cluster structure can be characterized in two stages. First, the O structure is defined. The skeleton of the oxygen atoms determines the shape of the cluster, the number of hydrogen bonds, and the hydrogen bond coordination of individual molecules. As an example, see a set of possible cluster shapes for $n = 20$, shown in Figure 1.

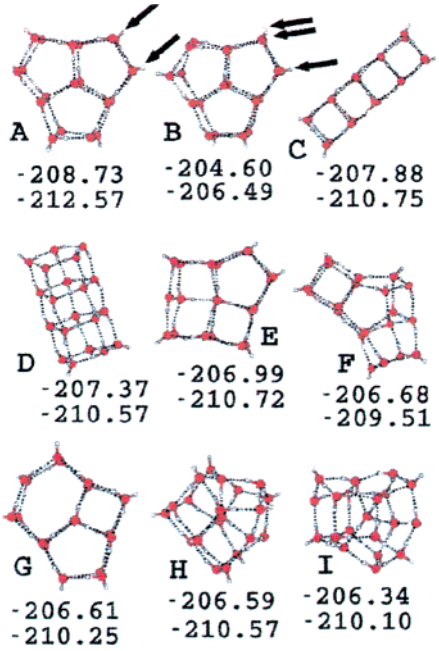

Figure 1. (A−H) Most stable structures of lowest energy families, found for $n = 20$: top energies, TIP4P; bottom energies, TTM2-R; in kcal/mol. Structure A appears to be the global minimum; it was reported in the past in refs 31, 36, and 47. Structure B corresponds to the same O-structure but includes three neighboring dangling H atoms (marked by arrows), which result in higher energy. Structure I was used as input for classical trajectories. All families except structure C were obtained in the course of the classical trajectory + HNI optimization protocol. Structure C was constructed by superimposing four-membered rings.

Another cluster feature is the H structure, that is, the position of the H atoms within the network of the hydrogen bonds. Each O structure is associated with numerous distinct potential minima, corresponding to different H structures. This multiplicity of H structures originates from the fact that an H atom may adopt one of two possible positions on a near neighbor O···O axis (i.e. it may be chemically bonded to either of the two O atoms). The number of unrestricted configurations would then be 2^K, where K is the number of hydrogen bonds. The allowed configuration space is however restricted by a constraint, that each O must be chemically bonded to exactly two H atoms. Even within this constraint, a multitude of H (or orientational) arrangements is possible. This multitude is a cluster analogue of the well-known orientational disorder (or "proton-disorder") characteristic of crystalline ice *Ih* and of the closely related ice *Ic* form, which was observed in nanocrystals.[71,72] It has been realized for a long time that different orientational arrangements in ice are nearly isoenergetic.[78−80] However, in clusters, energies of different H structures corresponding to the same O frame may differ significantly; this fact has been discussed in detail by Singer et al.[39] The broad energy range is largely a surface effect; specifically, the presence of neighboring dangling H atoms raises the cluster energy substantially, due to electrostatic repulsion. For example, for $n = 20$, the global TIP4P minimum corresponds to a "sandwich" structure with well separated dangling H atoms[36,47] (Figure 1A). The energy of a similar sandwich structure which includes two pairs of neighboring dangling H atoms (Figure 1B) is higher by several kilocalories per mole.

Structure optimization of water clusters is difficult because of the "rugged energy landscape", that is, a multitude of minima separated by high barriers. Moreover, a collection of water molecules which are brought in contact bond with each other

quite efficiently during simple minimization, and further structure optimization is associated with a relatively small energy gain, percentage-wise. One may note in this context that the latent heat of melting of ice *Ih* is only ~12% of the heat of sublimation. For the latent heat of crystallization of amorphous ice, literature values are of the order of 0.25 kcal/mol or less (i.e. ≤2% of the heat of sublimation[78]). Latent heats of phase transitions between different crystal ice forms are also of the order of ~1% of the heat of sublimation.[78]

Structure optimization of water clusters has been addressed in the past by a variety of approaches, including basin hopping,[22,36,37] evolutionary algorithms,[34,43,46,47] reaction coordinate analysis,[38] graph invariants,[81] the pivot method,[44] Gaussian density annealing,[30] and a diffusion equation scheme.[82]

The main aim of this study is to locate and characterize low energy structures of water clusters, for relatively large sizes (n = 48, 123, and 293). To the best of our knowledge, a detailed study of low lying minima for these sizes has been carried out for the first time. Parts of the computational scheme are specifically geared to the water cluster problem. The task is associated with formidable difficulties. One of them is the possible potential dependence of qualitative characteristics of low energy structures.[31,35,47,68] Due to the need to explore numerous minima of relatively large clusters, we employ the computationally efficient TIP4P potential.[69] For low lying minima of n = 21, and for select minima of other sizes, energy trends are double-checked against the polarizable TTM2-R potential.[83] While the gross energy trends appear consistent for the two potentials, there is still a distinct possibility of missing some important potential characteristic which affects the evolution with size.

Another problem pertains to incomplete sampling of the configuration space, especially for sizes corresponding to the onset of crystallinity. There are select cluster systems such as NaCl which crystallize easily in the course of the optimizations.[84] Unfortunately, H_2O does not belong to this category, most likely due to a high nucleation barrier. We are aware of only one simulation study in which water freezing was successfully obtained in a periodic boundary system, at a very high computational cost.[85] Here, a more limited approach is adopted, in an effort to bracket the size corresponding to the onset of crystallinity. Optimization is applied to initial structures cut out from a known crystal (ice *Ic*) and also to initially amorphous structures, and the results are compared. It is shown that for n = 48 and 123 the crystallinity is *lost* in the course of the optimization of initially crystal structures; moreover, final energies and structural characteristics are similar to those corresponding to amorphous initial conditions. On the other hand, for initially crystalline n = 293, the crystal structure of the cluster core survives the optimization, and the resulting final energy is lower than that of the optimized initially amorphous structures. These results are suggestive (although, of course, they do not constitute a conclusive proof) of the onset of crystallinity at a size of a few hundred molecules, in accord with spectroscopic evidence.[73]

Moreover, one may worry about missing "special" high symmetry cluster structures, which are different from ice *Ic* and which are hard to locate in a generic optimization code. For the size n = 48, a number of such structures can be guessed and constructed manually (a perfect "sandwich" of hexagonal rings and two kinds of tube structures). As discussed below, their energies are found to be higher than those of structures obtained in the optimization procedure; nevertheless, other, more favorable "special" minima cannot be ruled out.

Nevertheless, the subject of cluster structures in the tens to hundreds range is an interesting challenge, and it is hoped that useful insights can be gained. In section II the method and the calculations are presented. Section III describes the results. Summary and concluding remarks are presented in section IV.

II. Method and Calculations

A. Overview of the Optimization Scheme. Our general optimization strategy includes three stages. The first employs classical molecular dynamics (MD). Searching for low energy structures by classical trajectories is not a new idea; in fact, simulated annealing (i.e. gradual cooling by MD of an initially warm structure) has been among the first tools applied. The well-known problem is trapping of annealing trajectories in high energy minima. Here, we employ a variant which proved to be surprisingly effective. A set of relatively long classical trajectories is run at different energies, corresponding to temperatures in the range 100−200 K. Structures along the trajectories are minimized at constant intervals (see Figure 2, for n = 123). At low temperatures, molecular mobility is limited, and only minima in the vicinity of the initial structure are accessed. In the high temperature regime the system is mobile and probes numerous minima; however, high energy structures are preferred. There is some intermediate temperature range at which the mobilty is sufficient for effective exploration of the PES; however, low potential energy regions are still accessed preferentially. In this range, classical trajectories "find" structures of particularly low energy (140 K for n = 123, Figure 2). These structures are collected and subjected to further optimization, as described below. To account for the existence of such an optimal temperature range for low energy minima, we recall the concept of phase coexistence in clusters, introduced by Berry et al.[86]

In the second stage, optimization of H structures is carried out for low energy minima found by classical trajectories. A Monte Carlo (MC) process is used which probes different orientational arrangements, for a given O structure. This procedure is needed, since typically the trajectories do *not* produce an optimal H structure for energetically favorable O frames. In particular, the pattern of surface dangling atoms, which affects significantly the energetics, is optimized at this stage. The MC algorithm was adopted from refs 80 and 87, which addressed orientational ordering in ice.

The third step employs rigid body diffusion Monte Carlo optimization (RBDMC).[88] Diffusion Monte Carlo is a method to solve a time-independent Schrödinger equation by random walk of a cloud of replicas of a system.[89] In the long time limit, the distribution of replicas in space approaches the ground-state wave function. Here, RBDMC serves as a tool for structure optimization. Advantage is taken of the tendency of the replicas to drift toward low PES regimes. RBDMC is combined here with a computational device of PES smoothing, that is, replacement of the true potential energy by the energy of the nearby minimum, as in basin hopping algorithms.[36,90] The potential energy surface is thus smoothed to a sequence of flat-bottomed wells, and the potential barriers are eliminated. Such a smoothed PES was used by Wales and Hodges in conjunction with the classical Monte Carlo method, in a search for global minima of water clusters up to n = 21.[36]

B. The Potential and Other Computational Details. The computations described below are time-consuming, and therefore, the computationally efficient TIP4P potential[69] was used. TIP4P is a popular potential of the "three point charges plus Lennard-Jones" variety. TIP4P performs quite well for con-

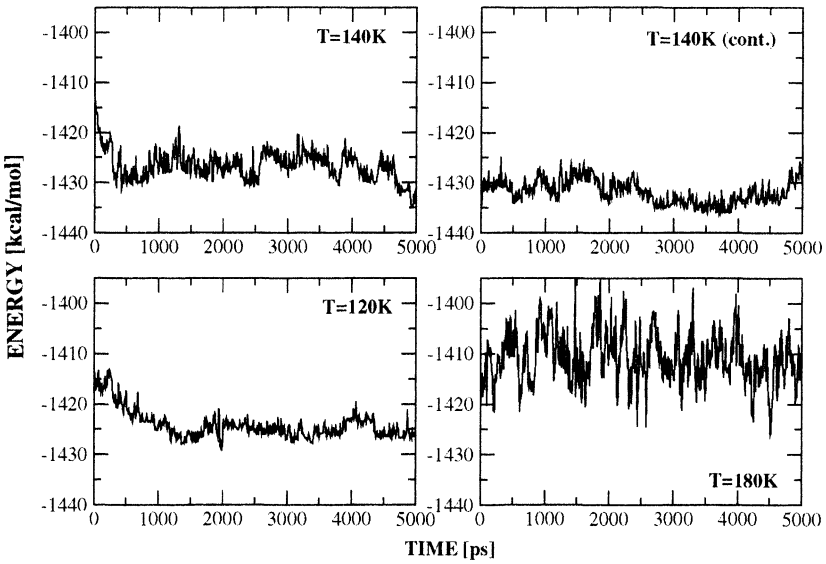

Figure 2. Potential energies of minima found along classical trajectories (in kcal/mol), as a function of time (in ps), at different temperatures, for $n = 123$. The lowest energy minima were found at $T = 140$ K.

densed phases and has also been used extensively in cluster calculations (see, e.g., refs 36, 38, and 47). However, the use of the choice of potential is a nontrivial issue. Energy spacing and ordering of cluster structures is known to be potential-dependent (e.g. refs 31, 35, 47, and 68). For large clusters, qualitative structural trends with size for stable minima appear to be of greater interest than identification of the exact lowest energy structure for a given potential. However, the possible dependence of these trends on the potential is a serious concern, as discussed in the past for the $n = 10-20$ size range.[31,47] In particular, Hartke[47] noted for $n = 20$ enhanced qualitative preference for "all surface" structures with TIP4P, as compared to the TTM2-F[70] potential, which favored low energy "centered cage" structures. A somewhat encouraging result of that study was the appearance of both types of structures in the low energy regime, for both potentials, albeit with different energy ordering. Thus, the use of TIP4P as a tool for searching for *candidates* for low energy structures appears reasonable, although checkup of the results with another, hopefully more accurate potential appears desirable.

At the present stage, TIP4P was employed in all the optimization steps, and unless stated explicitly otherwise, all energy results below pertain to that potential. Energies of select minima were recalculated with a polarizable TTM2-R potential,[83] which was calibrated against accurate ab initio results for $n = 2-6$ clusters and which yields good results for a variety of condensed phase H_2O properties. The performance of the two potentials is compared in more detail for $n = 21$; see section IIIA. Essentially, the general trends on the gross energy scale agree for both potentials, while there is clear disagreement in detailed energy ordering of the structures.

In all calculations, molecules were treated as rigid bodies. Classical trajectories employed the rigid body SHAKE algorithm,[91] while the minimization routine employed Euler angles. Minimizations were carried out with the help of a conjugate gradient routine. The stopping criterion was a reduction of the squared norm of the potential gradient vector by a factor in the range 10^{-11} to 10^{-14}. In the analysis of structures, two molecules were defined as hydrogen bonded if the O···O distance was less than 3 Å and the minimal O···H distance was less than 2.5 Å. A ring distribution program was adopted from a previous study.[92] We excluded from the statistics rings that are short-circuited by single hydrogen bonds (i.e. rings in which a pair of nonadjacent molecules was connected by a hydrogen bond).

C. Input Configurations. Preliminary effort was devoted to generation of input configurations for further optimization. Several methods were explored. In one, molecules were distributed at random within a cube of a preset size. In the second, rings of water molecules were stacked above each other at random; the size of the rings, in the range four to six molecules, was preset by the program, and some "random noise" was introduced to O···O distances, molecular orientations, and relative positions of ring centers. (This method was particularly useful for generation of tubelike configurations, such as the ones in Figure 1C and D.) In the third approach, structures were collected from classical trajectories for liquid droplets. The different structures were subjected to conjugate-gradient minimizations, and thus, a preliminary bank of configurations was generated.

One may note that for relatively small cluster sizes there is a high likelihood to find the global minimum already in the preliminary bank. Thus, in exploratory studies for sizes $n = 10-16$, the configuration bank included the lowest energy structures known from the study by Wales and Hodges.[36] For $n = 18$ and 19, the lowest energy bank structures were within 0.3 kcal/mol from the known lowest minima. For sizes of our interest, $n \geq 20$, the lowest energy structures were not found in the bank (although very lengthy random searches may have found them, at least for $n = 20-22$). For $n = 20-22$, the initial configurations used as input for further optimization were "generic-amorphous", from among the lowest energy structures obtained in random searches (see Figure 1I for $n = 20$).

For $n = 123$ and 293, a new set of input configurations was introduced, generated by "cutting out" structures from ice *Ic* crystals. Since a crystal sphere has an unphysically high surface energy, it was subjected to a short classical trajectory (a few tens of picoseconds) in the 150−180 K temperature range, to relax the surface, and subsequently minimized. Ice *Ic* was adopted as a starting point for these sizes, since it was observed in the past in electron diffraction studies of ice nanoparticles.[71,72] The aim was to observe if crystal structure survives the optimization process. Ice *Ic* corresponds to a nearly perfect tetrahedral bond network and is dominated by six-membered rings of water molecules. Its proton-disordered structure is

closely related to that of the common ice *Ih*. A description of the method to generate proton-disordered ice models can be found in ref 80.

Admittedly, the above choice of crystal input structures is biased by our knowledge of electron diffraction results. However, the objective was to find realistic low energy cluster structures rather than to actually observe crystallization of a liquid droplet to a correct crystal. For $n = 48$, both a structure derived from a crystal and a randomly generated "amorphous" structure were used as alternative inputs for the optimization procedure, for comparison. As discussed below, the resulting lowest energy structures corresponded to very similar energies, although the detailed shapes were different. For $n = 123$, the robustness of the final optimization result derived from the crystal structure was rechecked as follows. The structure was melted by heating to 220 K, subjected to a 5 ns trajectory, recooled, and used as a second input for the optimization procedure. As discussed below, the energy of the resulting optimized structure was very similar to the one obtained without melting and recooling, despite some structural differences. (The fact that the $n = 123$ structure melted during heating to 220 K is evidenced by different hydrogen bond lists in the two final structures. Figure 2 shows frequent transitions between high-lying minima already at $T = 180$ K.)

It will be shown below that, in the case of $n = 48$ and 123, the crystal core disappears during the optimization of the initial structures derived from ice *Ic*. However, the crystal core is retained for $n = 293$. An effort was made to recreate the low energy $n = 293$ structure by fully or partially melting it and recooling. This effort has been as yet unsuccessful, and the resulting structures corresponded to higher energies. The lack of success is not too surprising in view of a recent simulation study of water freezing (with periodic boundaries) which required very long trajectories lasting hundreds of nanoseconds.[85] In the present study, trajectories up to several tens of nanoseconds were used. Below, only the lowest energy structure derived from the crystal is discussed for $n = 293$.

D. Temperature-Dependent Classical Trajectories as a Tool for Structure Optimization. A set of 5 ns classical trajectories was run for each cluster size at different energies, corresponding to temperatures in the range 100−200 K. The exception was $n = 293$, for which shorter 500 ps trajectories were used, because of the significant computer time requirement. Structures along the trajectories were minimized every 10 ps. At temperatures at which particularly low energy structures were found, the trajectories were further extended by a factor 2−5. The energies of the lowest energy structures found at different temperatures are given in Figure 3. The energies of minima along individual trajectories are shown in Figures 2 and 4, for $n = 123$ and 20. It is seen that, at temperatures at which lowest energy structures are found, the system is characterized by substantial long time fluctuations of the potential, corresponding to motions within different "mega-basins". Therefore, relatively long trajectories are required to find low energy minima, and different portions of a given long trajectory may correspond to substantially different minimum energies (see the two 140 K plots in Figure 2). For $n = 48$, 123, and 293, temperatures corresponding to the lowest energy minima were obtained at 160, 140, and 160 K, respectively (Figure 3). To double-check the $n = 123$ result, the final structure of the 220 K trajectory was recooled to temperatures in the 130−150 K range and additional 5−10 ns trajectories were run in this range. The lowest energy minima obtained at 140 K and 145 K were of very similar energy as the one obtained originally at 140 K.

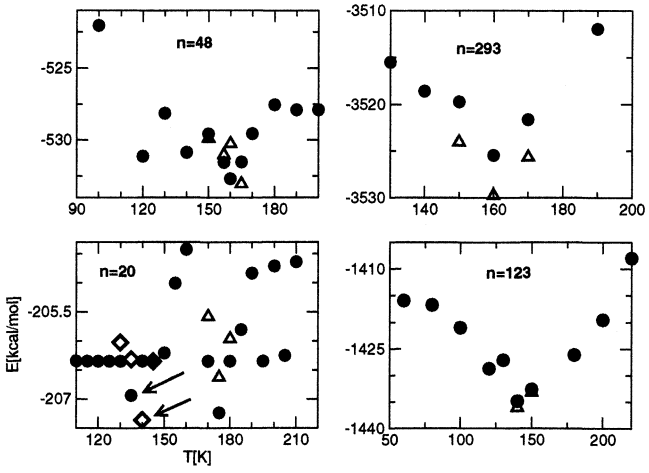

Figure 3. Energies of the lowest energy structures, as a function of temperature, obtained in classical trajectories for $n = 20$, 48, 123, and 293: black circles, structures from the initial 5 ns runs; triangles, a 5 ns continuation; diamonds, a 25 ns continuation. Arrows denote "sandwich" $n = 20$ structures. For $n = 293$, shorter trajectory stretches of 0.5 ns length were used. For $n = 20$ and 48 initial configurations were obtained in a random search. For $n = 123$ and 293 the starting point was a spherical shape cut out from the ice *Ic* crystal.

The optimal temperature for accessing low lying minima is related to barrier heights of transitions leading toward such minima. Investigation of barrier heights is outside the scope of the present study. However, some estimates can be made. As a lower bound for typical barrier heights, one can take energy differences between visited minima—of the order of several kilocalories per mole (see Figure 2 for $n = 123$). As an estimate for an upper bound, one can adopt the amplitude of fluctuations in the total kinetic (or potential) energy during the trajectory; the amplitude is ∼6 kcal/mol for $n = 48$, increasing to ∼15 kcal/mol for $n = 293$. (As the cluster size increases, the fraction of total energy that can be mobilized for a transition decreases.) These estimates are similar to barrier heights calculated for transitions between inherent structures of TIPS2 liquid,[93] which were mostly in the range 0−8 kcal/mol, with rare transitions corresponding to much higher (20 kcal/mol) values.

It should be noted that the temperatures in Figures 2−6 denote that value to which the initial structure was heated before starting the run. Energy rather than temperature is conserved along classical trajectories. The temperature undergoes substantial fluctuations, especially for the smaller clusters.

For the smaller clusters $n = 20$−22, more irregular behavior was obtained for the minimum energies as a function of temperature than for the case of the larger clusters. Figures 3−5 display the results for $n = 20$. The sandwich structure was accessed only at $T = 135$ K and 140 K. Its energy was somewhat higher than that of the global minimum (Figure 1A), because of the somewhat less favorable H arrangement. Figure 5 shows the dissimilarity index of the minima along the trajectories with respect to the initial "amorphous" structure (Figure 1I) and the sandwich. The dissimilarity index (DSI) is defined in the Appendix; low dissimilarity index corresponds to high similarity. It is seen in Figure 5 that at 110 K the trajectory remained in the vicinity of the initial structure, apparently due to low molecular mobility. At 135 K, the middle section of the trajectory approached the vicinity of the sandwich structure. However, during most of this time, the minima corresponded to strongly distorted sandwich structures, and only during relatively short intervals, was a perfect sandwich shape accessed (at intervals corresponding to the lowest energy and the lowest

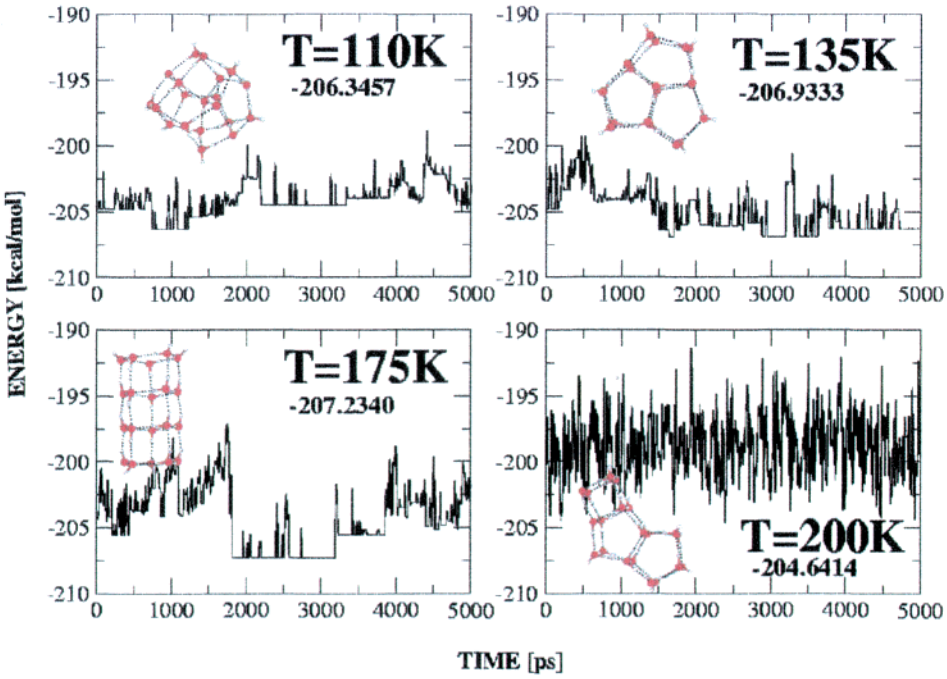

Figure 4. Potential energies (in kcal/mol) of minima found along classical trajectories, as a function of time (in ps), at different temperatures for $n = 20$. The inset shows the lowest energy structure found in a given stretch of a trajectory.

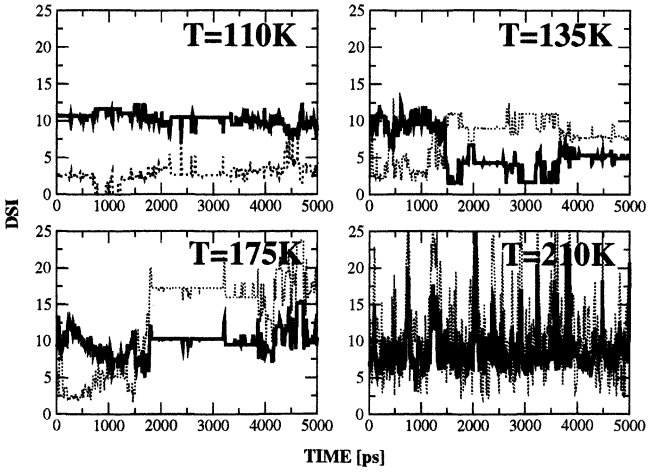

Figure 5. For the $n = 20$ minima found along the same trajectories as those in Figure 4, dissimilarity index to a sandwich structure (solid line), and to the initial "quasi-spherical" structure (dotted). High similarity corresponds to a low dissimilarity index.

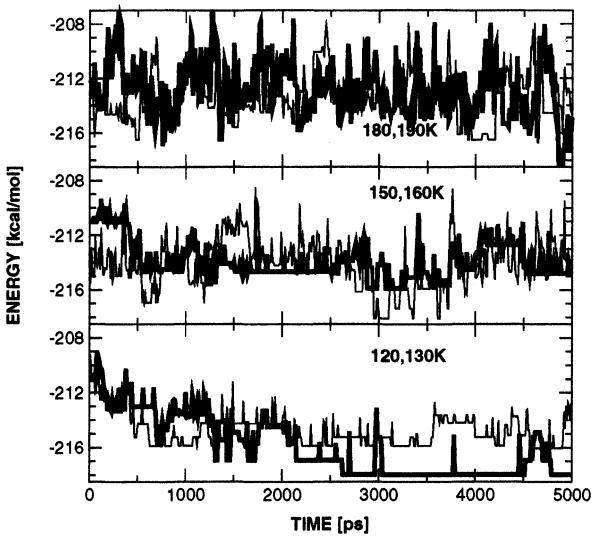

Figure 6. Potential energies (in kcal/mol) of minima found along classical trajectories, as a function of time (in ps), at different temperatures, for $n = 21$. The thin line in each panel refers to the higher temperature.

DSI within the 1500−3600 ps section of the trajectory; see Figures 4 and 5). The plot of the minimum energy as a function of temperature for $n = 20$ (Figure 3) displayed a second dip at 175 K. At this temperature, the trajectory froze temporarily to another ordered structure, a pentagonal pipe (Figure 1D). Interestingly, the "cubic" pipe (Figure 1C), which is only ∼1 kcal/mol above the global minimum, was never accessed in the trajectories.

For $n = 21$, a preferred temperature for accessing low energy structures was not obtained; the minimum energy value was found to oscillate between −216 and −218 kcal/mol in the 120−200 K range (Figure 6). Structures of energy close to −218 kcal/mol were found at several temperatures; this energy is only slightly above that of the most stable structure known for $n = 21$ in TIP4P (−219.19 kcal/mol[36]). The behavior of minimum energies as a function of trajectory time for $n = 21$ is instructive (Figure 6). The 120 K trajectory "finds" a low energy structure and remains there; as opposed to a 130 K trajectory, which keeps moving in a higher energy regime. Most of the minima probed by the 150 and 160 K trajectories are in the same energy range as the 130 K ones, but the transitions between minima are more frequent, and the range of energy fluctuations is larger. The 160 K trajectory undergoes several quick visits to the vicinity of the low energy minima at −218 kcal/mol. For the 180 and 190 K trajectories, the range of energy fluctuations is even larger, but the mean energy increases as well. Still, a short visit to a low energy minimum is observed in one of the trajectories. Apparently, for larger clusters such visits become improbable at these temperatures.

For $n = 22$, trajectories in the 120−190 K range resulted in the lowest energy structures within only 0.7 kcal/mol from the energy of the initial structure, which was located in a random search (at −228.5357 kcal/mol). As seen in Table 1, for this

cluster more substantial energy gain was obtained at further stages of the optimization.

Table 1 shows the energy gain with respect to the initial structures for the different cluster sizes, obtained during the MD optimization stage. For $n = 48-293$, the energy decrease was in the range 16−37 kcal/mol. For $n = 20-22$, the minimization of trajectories brought the structures within 1−2 kcal/mol from the known lowest energy minima.

E. Hydrogen Network Improvement (HNI). At this stage, select low energy structures obtained in the trajectories were subjected to H structure optimization. For this purpose, a Monte Carlo (MC) procedure was implemented, which is closely related to the one used in past studies of orientational energetics in ice.[80,87] In each MC step, a change of the cluster H structure was attempted, for a given O frame. The trial step, designed to avoid disruption of the H-bond network, was constructed as follows. First, a chain of unidirectional hydrogen bonds OH···OH···OH···OH was located at random, and the direction was switched by relocating H atoms to neighboring molecules (as in O···HO···HO···HO···H). To ensure proper termination, the chain must close on itself to a loop. Alternatively, it may be open, terminating at the cluster surface. Specifically, it may be terminated by a dangling O atom on one side and a dangling H atom on the other; in that case, during the MC step the dangling H atom is moved to the other side of the chain, as in HO···HO···HO···HO. (It may be seen from the different cluster models that their surfaces abound in dangling, that is, undercoordinated, H and O atoms. Inclusion of the "open" chains in the MC run is necessary to probe different dangling atom configurations, which influence significantly cluster energetics.[39])

The new structure resulting from switching of the chain direction was then subjected to reminimization. Reminimization is necessary to calculate accurately the energy difference between the new and the old H structures. Although the O frame is usually retained during an MC step, the corresponding minimum geometry changes slightly; the result is substanial energy relaxation. Sometimes the O structure is also altered during the minimization. The energy difference between the initial and the final minimum energy structures is used to determine the acceptance probability of the new H configuration, according to the usual Metropolis prescription. Temperatures in the range 1−175 K were tried in the MC simulations; best results were obtained typically at 1 K.

The results of HNI are shown in Table 1. For $n = 20-22$, energy improvement was of the order of 1 kcal/mol, which in the case of $n = 20$ and 21 was sufficient to reach the presently known global minima for these sizes.[36] For $n = 48$ and 123, HNI resulted in energy lowering up to several kilocalories per mole, while, for $n = 293$, an energy gain up to ∼13 kcal/mol was obtained. It is noted that the energy ordering of structures may be changed by HNI, and the lowest energy structure obtained from HNI is not necessarily derived from the most stable structure obtained in MD. In one of the $n = 48$ calculations, RBDMC optimization was applied before the HNI protocol. In that case the energy gain due to HNI was a modest fraction of a kilocalorie per mole, suggesting that DMC contributes to H as well as O structure optimizations (see below).

The obvious concern is the convergence, that is, whether the lowest energy H structure is in fact found in the above procedure. The procedure seems to be highly effective at gross structural adjustments, most notably at removal of "bad" (i.e. adjacent) dangling H pairs, which are associated with high energy. However, after removal of the latter, there is still a large number of possible H arrangements, which are very close in energy. These numerous structures are a cluster equivalent of the "proton disorder" prevalent in ice, that is, a macroscopic number of approximately degenerate H arrangements consistent with the ice O structure. We cannot be certain that HNI procedure locates the lowest energy H arrangement from among the low energy manifold; however, the possibility of a significant additional energy gain due to H-bond optimization appears unlikely.

F. Diffusion Monte Carlo Optimization. The basic DMC algorithm[89] is a numerical method to find the ground state of a quantum system. DMC relies on the fact that, upon the substitution $t' = it$, the Schrödinger equation is converted to a diffusion equation; the kinetic energy operator represents the diffusion term, and the potential energy represents the source/sink term. The basic description of the algorithm can be found in refs 89 and 94. The ground state of the system is obtained in DMC from a random walk of numerous replicas of the system according to the diffusion equation. In the long time limit, the distribution of the replicas in space approaches the ground-state wave function. The rigid body version of DMC[88] employs as MC steps random translations and random rotations of rigid molecules.

Here, RBDMC[88] is used as an optimization tool (DMCOPT), relying on the tendency of the replicas to explore low energy regions of the PES. Since the true vibrational ground state of the system is *not* the target, simulation parameters are readjusted to facilitate exploration of the configuration space. First, the PES is smoothed employing a "basin-hopping" method that was used in the past in conjunction with classical Monte Carlo[36,90] and classical trajectories.[37] The true PES at a given system configuration is replaced by the energy of the nearby minimum. Second, atomic masses were varied to improve the performance. Very light atomic masses result in large Monte Carlo steps and facile exploration of the configuration space; however, the drift toward low potential energy regions is lost (due to "high zero-point energy"). Large masses result in trapping in local minima. The best results were obtained by setting the O atom mass close to that of the H atom.

A DMCOPT cycle consisted of several hundred RBDMC steps, run for 100−500 replicas. The current version of the program enables parallel runs on a PC cluster, which effectively multiply the number of replicas by the number of the available processors (in our case up to 12). At the end of each cycle, several tens of lowest energy configurations accessed during the simulation are replicated and used as input for the next cycle. DMCOPT is currently tested as an independent optimization tool, to be applied without preliminary MD-HNI calculations. While the method is computationally intensive, minima of energy similar to those for the full MD-HNI-DMCOPT procedure were obtained for $n = 20$, 21, 48, and 123; these results will be discussed separately.[95]

In the present application, DMCOPT runs were aimed at improving the results of the MD-HNI procedure. That is, a collection of best structures obtained in MD-HNI was replicated and used as input for several DMCOPT cycles. Energy lowering was in fact obtained for $n = 22$ (by 0.5 kcal/mol) and for 48 (by 2 and 5 kcal/mol, respectively, in two separate simulations; see Table 1). For $n = 123$, no improvement was obtained in DMCOPT with respect to the best MD-HNI result. One of the reasons for this disappointing behavior may be the rigidity of the cluster; that is, the cluster interior allows for a very limited space for movements of water molecules. Large steps (typical of a small mass-scaling factor) result in interpenetration of

TABLE 1: Lowest Energies (in kcal/mol) Obtained in Different Optimization Stages

n	init[a]	MD[b]	HNI[c]	DMC[d]
20	−206.35	−207.36	−208.73	
21	−209.06	−218.59	−219.19	
22	−228.54	−229.23	−230.62	−231.12
48[e]	−503.21	−534.09	−536.65	−539.10
48[f]	−517.07	−533.04		−536.32
			−536.58	−538.24
123	−1409.33	−1436.06	−1440.61	
123[g]	−1398.64	−1435.73[h]	−1438.72	
293	3495.22	−3529.74	−3541.46	

[a] Input structure for the optimization. [b] Lowest energy structure obtained in classical trajectories. [c] Lowest energy structure obtained after application of HNI; it is derived from one of the low energy structures obtained in the trajectories, but not necessarily the lowest one. [d] Lowest energy structure obtained after subjecting previously collected low energy structures to DMC optimization. [e] Initial structure was cut out from a crystal. [f] Initial structure was generated by a random search. DMC was run using trajectory structures as input, followed by HNI and another DMC optimization. [g] Input structure: minimized last structure of the 5 ns trajectory at 220 K. [h] Lowest energy structure was obtained in a 145 K trajectory.

TABLE 2: Changes in Cluster Properties during Different Stages of the Optimization Scheme for $n = 48$[a]

property	init	MD	DMCOPT+HNI
energy	−517.07	−533.04	−538.24
NHB	86	86	86
NDH	10	10	10
NBDH	6	2	0
NCN(2)	1	3	1
NCN(3)	20	14	18
NCN(4)	25	31	29
NCN(5)	2	0	0
NR(3)	0	0	0
NR(4)	19	15	12
NR(5)	22	29	31
NR(6)	21	23	23
E(I)	−428.86	−425.14	−452.03
E(II)	−55.89	−63.80	−61.90
E(III)	−25.83	−31.04	−19.62
E(IV)	−6.48	−13.06	−4.69

[a] The initial structure was obtained from a random search. The energies in kcal/mol correspond to the lowest minima obtained at each stage. NHB, NDH, and NBDH denote the numbers of hydrogen bonds, dangling hydrogens, and "bad" dangling hydrogens, respectively. NCN and NR correspond to numbers of molecules of different coordinations (2−5), and rings of different sizes. *E*(I−IV) are energy contributions from different interaction ranges, for O−O distances of <3, 3−5, 5−7, and >7 Å between interacting molecules.

molecules, yielding high repulsion energy and minimization problems. The surface of the cluster is much more flexible, and small steps (required for the numerical stability of the interior) are usually too small to significantly explore the space of low energy configurations. Modifications are indicated, such as multiple step sizes, or separate optimization cycles for surface and interior.

G. Structural Changes during Optimization. Table 2 shows the evolution of the structural properties of the "best" (i.e. lowest energy) minima obtained during different stages of optimization, for $n = 48$. The initial structure was taken from the random search bank. It is seen that in the course of the optimization the energy decreased by a total of 21 kcal/mol (16 kcal/mol during the MD stage and a further 5 kcal/mol during DMCOPT + HNI). *Note that this energy lowering occurred without a change in the number of hydrogen bonds!* The following changes occurred during MD optimization: "Bad" dangling H atoms (i.e. pairs of dangling H atoms belonging to hydrogen bonded water molecules) were eliminated. The number of five-membered rings increased. Second near-neighbor and longer range interactions *E*(II−IV) were optimized at the expense of some deterioration in the near-neighbor interaction *E*(I). During further DMCOPT + HNI optimization, an opposite trend was observed: the quality of hydrogen bonds (i.e. *E*(I)) improved substantially at the expense of the longer range interactions. Both optimization stages were associated with the decrease in the number of small strained four-membered rings of water molecules.

TABLE 3: Changes in Cluster Properties during Different Stages of the Optimization Scheme for $n = 293$[a]

property	init	MD	MD′	HNI
energy	−3495.22	−3529.74	−3529.17	−3541.46
NHB	551	555	554	555
NDH	35	31	32	31
NBDH	2	2	0	0
NCN(2)	8	3	3	2
NCN(3)	60	61	63	65
NCN(4)	219	224	222	219
NCN(5)	6	5	5	7
NR(3)	1	1	0	0
NR(4)	46	51	53	52
NR(5)	114	120	116	121
NR(6)	254	250	252	249
E(I)	−2859.07	−2891.10	−2874.69	−2886.34
E(II)	−480.03	−463.05	−473.74	−485.72
E(III)	−131.98	−147.53	−148.28	−140.49
E(IV)	−24.14	−28.06	−32.46	−28.91

[a] The energies in kcal/mol correspond to the lowest minima obtained at each stage. MD denotes the lowest energy structure obtained from the trajectories. MD′ denotes that trajectory structure which yielded the lowest energy structure after HNI. NHB, NDH, and NBDH denote the numbers of hydrogen bonds, dangling hydrogens, and "bad" dangling hydrogens, respectively. NCN and NR correspond to the numbers of molecules of different coordinations (2−5), and rings of different sizes. *E*(I−IV) are energy contributions from different interaction ranges, for O−O distances of <3, 3−5, 5−7, and >7 Å between interacting molecules.

Table 3 displays structural evolution during the optimization of $n = 293$. In this case, the initial structure was constructed by cutting out a spherical shape from cubic ice, followed by limited surface relaxation (see discussion of initial structures above). As noted before, the open crystal structure is not particularly favorable for the surface. Therefore, during the optimization, structural changes occurred predominantly at the surface, which moved *away* from the crystal structure. The energy decrease was 46 kcal/mol, out of which 34 kcal/mol were obtained in MD, and the rest in HNI. During the optimization, the number of hydrogen bonds increased by 4. Moreover, optimization was associated with an increase in the number of four- and five-membered rings, a decrease in the number of six-membered rings (characteristic of the crystal), elimination of most of the two-coordinated molecules, and overall lowering of all interaction components. Note the decrease in short range interactions *E*(I) and *E*(II), at the expense of longer range interactions, during HNI. In addition to the formation of one new hydrogen bond, this result is likely to be associated with reshuffling of the surface dangling atom pattern.

H. Tests for the $n = 20-22$ Range. In studies of cluster energetics, dependence on the potential is a major concern, as discussed, for example, in refs 31, 35, 47, and 68. As explained in section II.B, TIP4P was employed during the optimization, due to its computational efficiency. Subsequently, select low lying minima were recalculated with the polarizable TTM2-R.[83] Figure 7 shows a comparison of minimum energies for TIP4P and TTM2-R, for 131 different structural families of

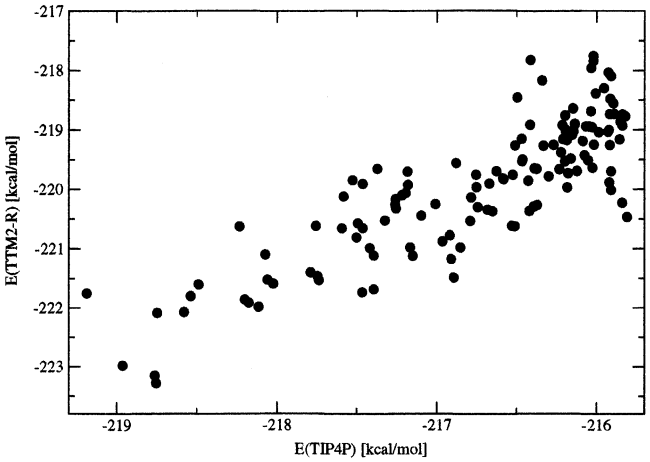

Figure 7. Comparison of minimum energies for TIP4P and TTM2-R potentials, $n = 21$. Each point corresponds to a single structure, minimized with two potentials. Results are shown for a collection of lowest energy structures obtained with TIP4P for 131 different structural families.

$n = 21$. It is seen that the energy trends are similar for the two potentials; however, detailed ordering of the minima, on the scale of a few kilocalories per mole, differs considerably. Still, despite the scatter of the points, there is a clear correlation between TIP4P and TTM2-R energies. Consistent results can be seen in Figures 1 and 8−11, which show low energy structures for different cluster sizes. Again, on the scale of a few kilocalories per mole, the energy ordering differs considerably for the two potentials. However, structures which correspond to substantially higher TIP4P energies than those for the lowest energy ones do so for TTM2-R as well. While TTM2-R is likely to be more accurate than TIP4P, we suspect that none of the presently available empirical or ab initio models are sufficiently accurate to predict the exact energy ordering in this size range. We are encouraged by the fact that "gross" trends appear consistent for both potentials. It remains to be hoped that the evolution of general structural features with size obtained with TIP4P optimizations is correct.

The low energy configurations for $n = 20$ are shown in Figure 1. For that size, three highly ordered structures are possible—a sandwich, a four-membered tube, and a five-membered tube. The sandwich is the lowest energy structure found for both potentials, in accord with past studies.[36,47] Addition of one molecule alters significantly the energetics (Figure 8). The most "regular" low energy $n = 21$ structure found (B) is a three-layered sandwich of five + four fused rings. Structure C is rounded, with a four-coordinated molecule at the center; structures A and B are flatter. Structure A was reported in the past as the TIP4P global minimum.[36,47] Structures A−D are nearly isoenergetic in both potentials. Two somewhat higher energy structures E and F are derived from ordered low energy $n = 20$ structures, by insertion of a molecule into one of the edges.

For $n = 22$ (similarly to $n = 21$) we find a number of low energy structures of quite different shapes, within a narrow energy range (Figure 9 A−D). As discussed in ref 47, this size range is characterized by the appearance of low energy three-dimensional structures with a "core" of an internal four-coordinated molecule (such as minimum C), in addition to "all surface" cluster configurations (such as A−B). Structure D represents a borderline case in which the "internal" molecule is close to the surface. Structure B was found in the past in ref 47. In that study, two additional low energy structures were reported, which appear to be different from A, C, or D. The

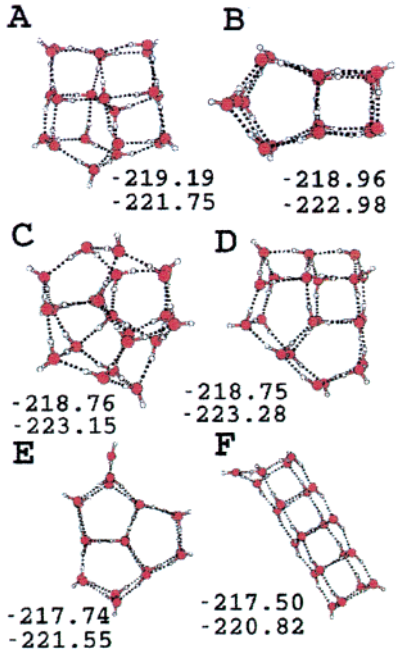

Figure 8. Structures for $n = 21$: top energies, TIP4P; bottom energies, TTM2-R; in kcal/mol. (A−D) Most stable structures of the lowest energy families, found for $n = 21$ using the TIP4P potential. (E and F) Higher energy, "interesting" structures. Structure A appears to be the global TIP4P minimum, reported in the past in refs 31, 36, and 47. Structures A and C−E were found during a MD-HNI-DMCOPT optimization sequence. Structures B and F were constructed by combining water rings. Structure B consists of three nearly planar layers.

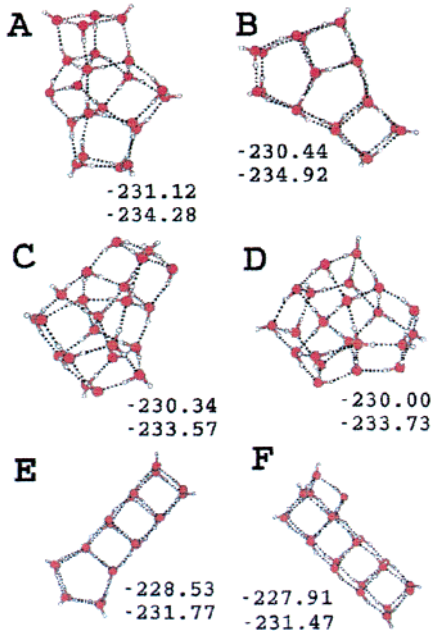

Figure 9. Structures for $n = 22$: top energies, TIP4P; bottom energies, TTM2-R; in kcal/mol. (A−D) Most stable structures of lowest energy families, found for $n = 22$ in the MD-HNI-DMCOPT optimization sequence. (E and F) Higher energy, "interesting" structures, constructed by combining water rings.

lowest energy TIP4P structure reported in ref 47 is of a centered cage variety, of energy between those of A and B; that structure was also proposed as a TTM2-F global minimum.

The fact that our study and that of ref 47 located different lowest energy TIP4P structures for $n = 22$ should not be very surprising. These results suggest that, starting from the size of tens of molecules, low energy cluster structures located in

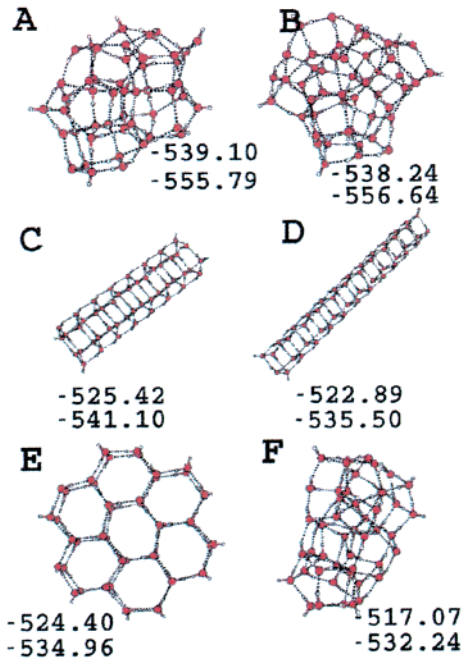

Figure 10. Structures for $n = 48$: top energies, TIP4P; bottom energies, TTM2-R; in kcal/mol. (A) Lowest energy structure found in TIP4P; crystal initial conditions were used. (B) Lowest energy structure found in TIP4P using as input amorphous structure F, which was obtained in a random search. The ordered structures C−E were constructed manually and did not appear during the optimization sequence.

different studies, or different optimization runs, may be quite irreproducible; there are just too many distinct structures of similar energies. Investigation of general structural characteristics of low energy cluster structures is likely to constitute the most meaningful objective.

III. Results: Optimized $n = 48$, 123, and 293 Structures—Trends with Size

The low energy structures for the sizes of our main interest, $n = 48$, 123, and 293, are shown in Figures 10−12. Evolution of structural properties with size, for low energy structures, is displayed in Figures 13−15 and in Table 4. In this size range, the shapes of the low energy structures can be described as "three-dimensional compact", lopsided for $n = 48$, more rounded for $n = 123$, and becoming nearly spherical for $n = 293$. The majority of molecules are four-coordinated. There is however a substantial population of three-coordinated H_2O, decreasing from ∼40% to ∼20% as the size increases from $n = 48$ to $n = 293$. A small number of two- and five-coordinated molecules can be found in the structures as well. The energy per molecule of the lowest energy TIP4P structures decreases from −11.23 to −11.71 and −12.09 kcal/(mol H_2O), respectively, for $n = 48$, 123 and 293. These values are still far from the minimum TIP4P energy calculated for ice *Ic* (−13.64 kcal/mol/H_2O) and ice *Ih* (−13.65 kcal/mol/H_2O).[80]

Not surprisingly, the three-coordinated molecules are concentrated at the outer surface (Figures 13 and 14). Comparison to a crystal is of interest. A perfect hexagonal surface of the ice *Ih* (0001) or ice *Ic* (111 surface) is puckered, with the lower half of the surface bilayer four-coordinated and the upper half (∼1 Å above) three-coordinated (see, e.g., Figure 2.3 of ref 79). Each three-coordinated molecule is bonded to three four-coordinated H_2O molecules below it. While the molecular structure of the cluster surfaces is noncrystalline, one can still

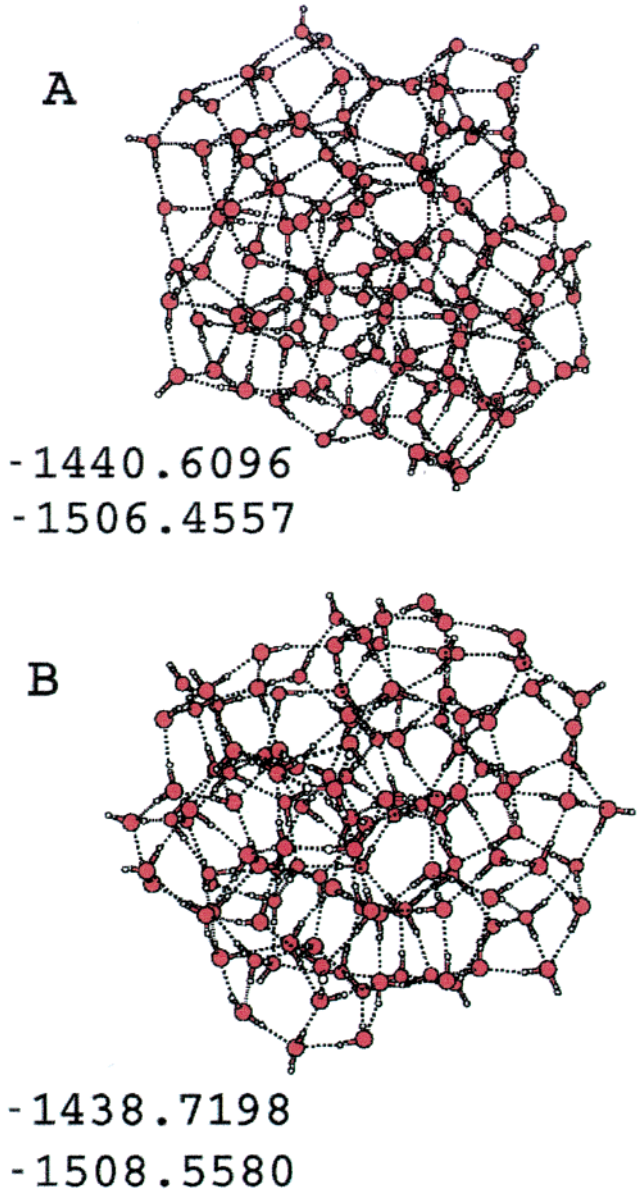

Figure 11. (A) Lowest energy structure found for $n = 123$, in TIP4P (−1440.61 kcal/mol), for crystal initial conditions. (B) A nearly isoenergetic structure, obtained after melting the cluster, recooling, and subjecting it again to the optimization procedure. Top energies: TIP4P. Bottom energies: TTM2-R; in kcal/mol.

see in the models in Figures 10−12 three-coordinated molecules protruding from the surface. Moreover, the distance-dependent coordination distributions (Figure 14) display an outer surface peak for three-coordinated molecules and an inner surface peak for four-coordinated ones. Interestingly, the relative ratio of the two peaks decreases with increasing size and becomes significantly less than one for $n = 293$ (in contrast to the case of the crystal surface, for which this ratio is exactly 1). The deficiency of three-coordinated molecules in the ice nanoparticle surfaces has been noted in the past, on the basis of the analysis of the infrared spectra.[73] It appears that curved surfaces allow for enhanced population of fully coordinated molecules (albeit with a distorted coordination shell), as compared to the case of a flat crystalline surface.

Water rings are an important structural feature of H_2O containing systems. For example, the structures of the low pressure crystal forms (ice *Ih* and *Ic*) are characterized by puckered six-membered rings, in conjunction with unstrained

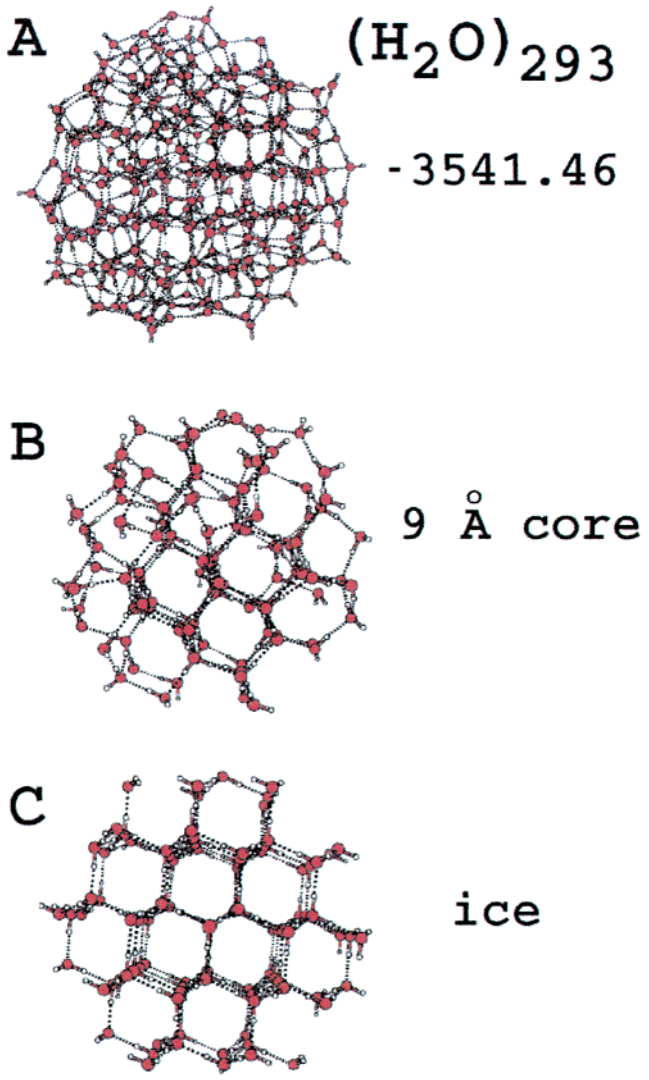

Figure 12. (A) Lowest energy structure found for $n = 293$ in TIP4P. (B) Largely crystalline core of the top structure, of radius 9 Å. (C) Crystal ice *Ic* structure, of radius 9 Å, shown for comparison.

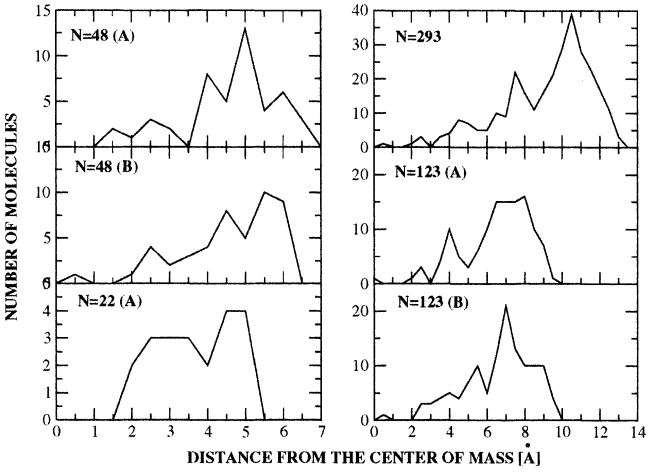

Figure 13. Distribution of molecular distances (in Å, measured from O atoms) from the cluster centers of mass, for the cluster structures shown in Figures 9−12.

nearly perfect tetrahedral coordination. In the disordered liquid water and amorphous ice phases, a broad ring distribution was demonstrated in simulations.[92,96] In clusters, the optimal structure constitutes a compromise between a trend for perfect tetrahedral

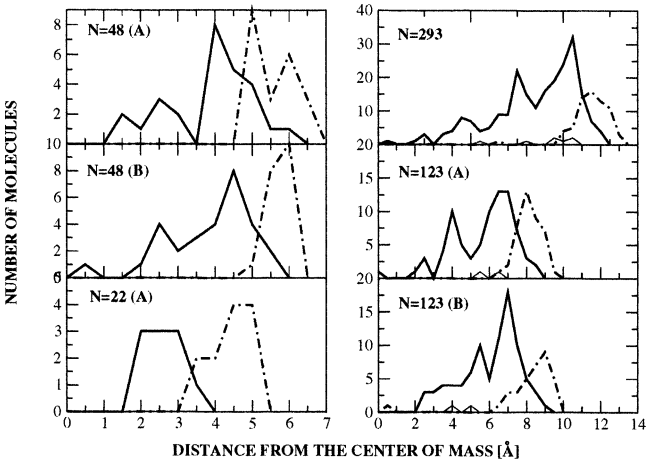

Figure 14. Distribution of coordinations, as a function of distance (in Å) from the cluster center of mass, for the cluster structures shown in Figures 9−12: thick solid lines, 4-coordinated molecules; dot−dashed lines, 3-coordinated molecules; thin-solid lines, 5-coordinated molecules.

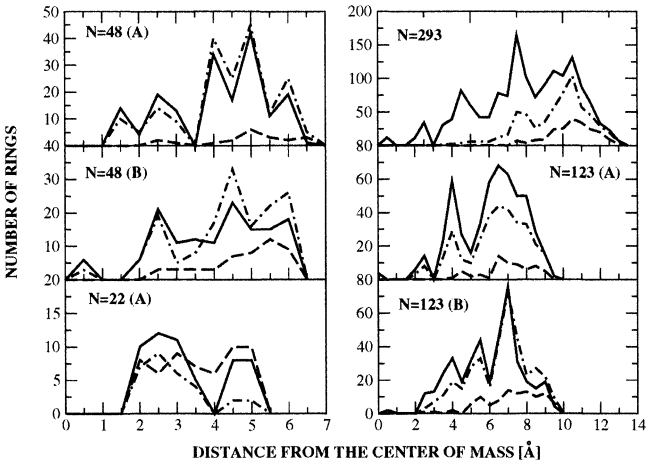

Figure 15. Distribution of ring sizes, as a function of distance (in Å) of a ring center to the cluster center of mass, the cluster structures shown in Figures 9−12: thick solid lines, six-membered rings; dot−dashed lines, five-membered rings; dashed lines, four-membered rings.

coordination (which favors six-membered rings) and a trend to eliminate surface dangling atoms and to increase the number of hydrogen bonds (which favors smaller rings). The relative importance of these trends depends on the surface-to-volume ratio and, thus, on size. A preference for small water rings in cluster surfaces was noted in the past in an investigation of the "tens of H_2O molecules" range.[38]

Ring distributions in clusters are shown in Table 4 and Figure 15. The distributions include four-, five-, and six-membered rings. Generally, the trend with increasing cluster size corresponds to increasing preference for the six-membered rings and reduction of the number of the strained four-membered ones. In $n = 22$, four-membered rings constitute the dominant species. All ring sizes in the range 4−6 can be found throughout the cluster, with larger rings concentrated preferentially in the inner part. For $n = 48$ and 123 we observe the development of the surface/core structure. In the external surface layer, a few angstroms thick, there is a comparable amount of five- and six-membered rings and a significant fraction of four-membered ones as well. In the interior of the $n = 48$ and 123 structures, the relative amount of four-membered rings is reduced; however, the amounts of five- and six-membered rings are still comparable. Thus, the cores of these cluster are noncrystalline, despite

TABLE 4: Change of Cluster Properties with Growing Cluster Size[a]

			%NCN				%NR			
n	NHB	%NDH	2	3	4	5	3	4	5	6
20[b]	34	15	0	60	40	0	0	67	33	0
21[b]	37	12	0	52	43	5	0	45	23	32
22[b]	38	14	0	55	45	0	0	48	21	31
48[c]	85	11	2	42	56	0	0	7	53	40
48[d]	86	10	2	38	60	0	0	18	47	35
123	226	8	1	33	65	2	1	9	39	51
123[e]	229	7	2	26	71	2	1	15	44	40
293	555	5	1	22	75	2	0	12	29	59
ice			0	0	100	0	0	0	0	100

[a] NHB is the number of hydrogen bonds, %NDH is the ratio of dangling hydrogens to all hydrogen atoms in the cluster, %NCN is the percentage of molecules with different coordination numbers (2−5), and %NR is the percentage of rings of different sizes. [b] Lowest energy TIP4P structures; see Figures 1, 8, and 9. [c] Structure A of Figure 10; initial structure cut from a crystal. [d] Structure B of Figure 10; a randomly generated initial structure. [e] Optimization applied after melting the initial structure and recooling.

the fact that the optimized $n = 48$A and $n = 123$A structures were derived from the crystal. (The second $n = 123$B structure was obtained from optimization after melting and recooling. Note the reduced number of six-membered rings in 123B as compared to 123A. The two structures are nearly isoenergetic; see Figure 11.)

The largest cluster investigated, $n = 293$, is characterized by an "amorphous" surface layer, including four-, five-, and six-membered rings, similar to those for $n = 48$ and 123. However, the next inner layer is already dominated by six-membered rings, despite some presence of five-membered ones, and further inside the cluster, the rings are almost entirely six-membered. A largely crystal core can be detected visually for this particle; see Figure 12. This is in contrast to the cases of $n = 123$A and B, for which visual inspection of the cores did not reveal traces of crystal structure.[97] Thus, our results are consistent with the onset of crystallinity in the $n = 100-300$ range.

For $n = 48$, several ordered structures, generated manually, were examined as well (Figure 10). In fact, this size was chosen since it allows for three such structures—perfect four- and six-membered tubes and a perfect sandwich composed of six-membered rings.[98] All these structures yielded significantly higher energies than the three-dimensional compact structure A; this result was double-checked with the TTM2-R potential. Sandwich structures such as E were proposed by Tanaka[42] to dominate the tens to hundreds of H_2O molecules size range, because of the high percentage of four-coordinated molecules, as compared to 3D structures. However, that study did not take into account surface relaxation of three-dimensional compact nanoparticles (such as A and B), which lowers the energy; see also ref 73. Thus, the number of hydrogen bonds in structures A and B (85 and 86) is slightly higher than that in the sandwich.[84] Moreover, in the sandwich, the large deviation of constituent molecules from the optimal tetrahedral bonding geometry destabilizes the structure. As already noted above, the quality of the hydrogen bonds, not only their quantitity, affects significantly the energetics.

IV. Summary and Concluding Remarks

The objective of this study has been to locate representative low energy structures of water clusters in the tens to hundreds of molecules size range. The optimization procedure included temperature-dependent classical trajectories, hydrogen network improvement, and optimization by DMC. There appears to be an optimal temperature range in which classical trajectories probe vicinities of especially low energy minima. Trajectories in this range were found to be a fairly efficient tool for locating structures of significantly lower energy than that of the initial one. However, the resulting orientational arrangements of water molecules within the hydrogen bond network are still not optimal. Therefore, an MC procedure was employed, designed specifically for their optimization. DMC-based optimization was found useful for final structural adjustment at some sizes ($n =$ 22 and 48); for larger sizes, further improvement of the method including multiple step sizes appears necessary. Cluster energetics is not simply determined by the number of hydrogen bonds, and improvement of the *quality* of hydrogen bonds plays an important role in the optimization.

Compact three-dimensional amorphous structures were obtained finally for $n = 48$ and 123. Such optimized structures were found starting from higher energy amorphous structures obtained in random search/liquid droplet simulations, as well as from initial structures which were cut out of crystal ice. This result is in qualitative accord with the measured IR spectra for the mean size $n \sim 100$, which matched the spectrum of amorphous ice.[73]

For $n = 293$, the lowest energy structure found includes a largely crystal core and an amorphous surface. The presence of a (strained) crystal core is in accord with past analysis of IR spectra in the pertinent size range.[73] The lowest energy structure for this size was derived from an initial configuration cut out of ice *Ic*. Optimization modified surface structure toward a more dense arrangement, associated with an increased abundance of four- and five-membered rings. Optimized structures employing melted configurations as a starting point corresponded to higher energies. We did not succeed in observing recrystallization of the melted $n = 293$ structures. This may not be very surprising, since trajectories lasting up to several tens of nanoseconds were used. Crystallization of supercooled water was obtained in a recent remarkable simulation study by Ohmine et al. with periodic boundaries in a trajectory lasting hundreds of nanoseconds.[85]

Presently, the study is being extended, to include cluster OH-stretch spectra. As noted above, OH spectra are an especially sensitive probe of the hydrogen bond network; schemes to derive cluster spectra from structures were developed by us in the past.[66,67,73] The recently available experimental data from collaborators include mean-size dependent FTIR spectra by the groups of Baerecker and Devlin,[73] and laser fragmentation spectroscopy by Buck et al.;[75] the latter technique provides information on infrared absorption by the cluster *surface*. The combined computational and experimental results will be presented elsewhere.[77] It is noted that the measured trends with size are reproduced by the calculations. The latter result is encouraging, considering the difficulties and the uncertainties of conformational searches for cluster sizes of our interest, such as possible potential dependence and the limited ability to sample the (huge) configuration space.

All the cluster structures shown in this study are available on request from the authors, via e-mail.

Acknowledgment. We thank Christian Burnham for the help with the TTM2-R potential. Paul Devlin, Udo Buck, and Sigurd Baurecker are acknowledged for helpful discussions.

Appendix. Comparing Clusters—Dissimilarity Index

One of the typical problems when searching for global/low energy minima of large molecular systems is a huge number of local minima (growing exponentially with the increasing system size). In consequence, storing and screening of *distinct* minima can be difficult. To reduce this problem, we divide structures into families and focus on the lowest energy structures of the different families.

A family is defined by its O-structure. A variety of criteria is possible to assess structural dissimilarity between two structures. The "dissimilarity index" (DSI) adopted here does not require overlapping of structures or matching of "nearly equivalent" atoms in the two structures. The DSI is calculated as follows: A set of O···O distances (including non-nearest neighbors) is calculated for each structure. The distances are sorted in decreasing order. The two sets of distances are defined as vectors (V_1 and V_2) of dimension $n(n-1)/2$. The DSI between the two structures is defined as $|V_1 - V_2|$, that is, the Euclidean distance between two points defined by these vectors.

One still has to check manually, for each n, which DSI values refer to the same family (with slightly distorted oxygen positions) and which indicate different families. Already for clusters with ~20 water molecules, it is a nontrivial task to recognize visually different families (except in special, well-defined cases). In the cases of $n = 48$, 123, and 293, the idea of "distinct families" is no longer strictly applicable, since small changes (usually at the surface) may generate different families without significant distortion of the cluster shape. Still, coarse-grained DSI classification was found useful for division of numerous minima into a small number of distinct structural groups of significantly differing shapes.

References and Notes

(1) For example: (a) Vaida, V.; Tuck, A. F.; Goss, L. M.; Daniel, J. S.; Kjaergaard, H. *Abstracts of Papers, Part 2*, 218th National Meeting of the American Chemical Society, New Orleans, LA, Aug 1999; American Chemical Society: Washington, DC, 1999; 403-Phys. (b) Molina, M. J.; Tso, T. L.; Molina, L. T.; Wang, F. C. Y. *Science* **1987**, *238*, 1253. McCoustra, M. Rs. S.; Horn, A. B. *Chem. Soc. Rev.* **1994**, *23*, 195. Tielens, A. G. G. M.; Allamandola, L. J. In *Physical Processes in Interstellar Clouds*; Morfill, G. E., Scholet, M., Eds.: Reidel: Dordrecht, 1987.

(2) Fraser, G. T. *Int. Rev. Phys. Chem.* **1991**, *10*, 189.

(3) Scheiner, S. *Annu. Rev. Phys. Chem.* **1994**, *45*, 23.

(4) Chalasinski, G.; Szczesniak, M. M.; Cieplak, P.; Scheiner, S. *J. Chem. Phys*. **1991**, *94*, 2873.

(5) Gonzalez, L.; Mo, O.; Yanez, M.; Elguero, J. *THEOCHEM* **1996**, *371*, 1.

(6) Knochenmuss, R.; Leutwyler, S. *J. Chem. Phys*. **1992**, *96*, 5233.

(7) Van Duijneveldt-van de Rijdt, J. G. C. M.; van Duijneveldt, F. B. *Chem. Phys.* **1993**, *175*, 271; *Chem. Phys. Lett*. **1995**, *237*, 560.

(8) Kim, J.; Majumdar, D.; Lee, H. M.; Kim, K. S. *J. Chem. Phys*. **1999**, *110*, 9128; *Chem. Phys. Lett*. **1994**, *219*, 243.

(9) Kim, K.; Jordan, K. D.; Zwier, T. S. *J. Am. Chem. Soc.* **1994**, *116*, 11568.

(10) Jensen, J. O.; Krishnan, P. N.; Burke, L. A. *Chem. Phys. Lett.* **1995**, *241*, 253; **1995**, *246*, 13; **1996**, *260*, 499.

(11) Xantheas, S. S. *J. Chem. Phys*. **1994**, *100*, 7523; **1995**, *102*, 4505.

(12) Fowler, J. E.; Schaefer, H. F. *J. Am. Chem. Soc*. **1995**, *117*, 446.

(13) Kahn, A. *J. Phys. Chem.* **1995**, *99*, 12450.

(14) Estrin, D. A.; Paglieri, L.; Corongiu, G.; Clementi, E. *J. Phys. Chem.* **1996**, *100*, 8701.

(15) Khan, A. *Chem. Phys. Lett*. **1996**, *258*, 574.

(16) Kryachko, E. S. *Chem. Phys. Lett*. **1997**, *272*, 132.

(17) Pedulla, J. M.; Jordan, K. D. *Chem. Phys. Lett*. **1998**, *291*, 78.

(18) Guiang, C. S.; Wyatt, R. E. *Int. J. Quantum Chem*. **1998**, *68*, 233.

(19) Jiang, J. C.; Chang, J. C.; Wang, B. C.; Lin, S. H.; Lee, Y. T.; Chang, H. C. *Chem. Phys. Lett.* **1998**, *289*, 373.

(20) Chaban, G. M.; Jung, J. O.; Gerber, R. B. *J. Chem. Phys.* **1999**, *111*, 1823.

(21) Wales, D. J. *J. Chem. Phys.* **1999**, *111*, 8429.

(22) Day, P. N.; Pachter, R.; Gordon, M. S.; Merrill, G. N. *J. Chem. Phys.* **2000**, *112*, 2063.

(23) Stillinger, F. H.; David, C. W. *J. Chem. Phys.* **1980**, *73*, 3384. Weber, T. A.; Stillinger, F. H. *J. Phys. Chem.* **1983**, *87*, 4277.

(24) Plummer, P. L. M.; Chen, T. S. *J. Phys. Chem.* **1983**, *87*, 4190.

(25) Reimers, J. R.; Watts, R. O. *Chem. Phys.* **1984**, *85*, 83.

(26) Pillardy, J.; Olszewski, K. A.; Piela, L. *THEOCHEM* **1992**, *270*, 277.

(27) Farantos, S. C.; Kapetanikis, S.; Vegiri, A. *J. Phys. Chem*. **1993**, *97*, 12158.

(28) Eggen, B. R.; Marks, A. J.; Murrel, J. N.; Farantos, S. C. *Chem. Phys. Lett*. **1994**, *219*, 247.

(29) Wales, D. J.; Ohmine, I. *J. Chem. Phys.* **1993**, *98*, 7245; **1993**, *98*, 7257.

(30) Tsoo, C.; Brooks, C. L. *J. Chem. Phys.* **1994**, *101*, 6405.

(31) Sremaniak, L. S.; Perera, L.; Berkowitz, M. L. *J. Chem. Phys*. **1996**, *105*, 3715.

(32) Jung, J. O.; Gerber, R. B. *J. Chem. Phys.* **1996**, *105*, 10332.

(33) Fredj, E.; Gerber, R. B.; Ratner, M. A. *J. Chem. Phys.* **1996**, *105*, 1121.

(34) Niesse, J. A.; Mayne, H. R. *J. Comput. Chem.* **1997**, *18*, 1233.

(35) Pedulla, J. M.; Jordan, K. D. *Chem. Phys.* **1998**, *239*, 593; *Chem. Phys. Lett*. **1998**, *291*, 78.

(36) Wales, D. J.; Hodges, M. P. *Chem. Phys. Lett*. **1998**, *286*, 286.

(37) Li, Z.; Laidig, K. E.; Daggett, V. *J. Comput. Chem.* **1998**, *19*, 60.

(38) Baba, A.; Tanaka, J.; Saito, S.; Matsumoto, M.; Ohmine, I. *J. Mol. Liq.* **1998**, *77*, 95.

(39) McDonald, S.; Ojamäe, L.; Singer, S. J. *J. Phys. Chem. A* **1998**, *102*, 2824.

(40) Burnham, C. J.; Li, J.; Xantheas, S. S.; Leslie, M. *J. Chem. Phys.* **1999**, *110*, 4566.

(41) Dang, L. X. *J. Chem. Phys.* **1999**, *110*, 1527.

(42) Tanaka, H.; Yamamoto, R.; Koga, K.; Zeng, X. C. *Chem. Phys. Lett.* **1999**, *304*, 378.

(43) Qian, J.; Stockelman, E.; Hentschke, R. *J. Mol. Model.* **199**, *5*, 581.

(44) Nigra, P.; Kais, S. *Chem. Phys. Lett.* **1999**, *305*, 433.

(45) Egorov, A. V.; Brodskaya, E. N.; Laaksonen, A. *Mol. Phys.* **2002**, *100*, 941.

(46) Guimaraes, F. F.; Belchior, J. C.; Johnston, R. L.; Roberts, C. *J. Chem. Phys.* **2002**, *116*, 8327.

(47) Hartke, B. *Phys. Chem. Chem. Phys*. **2003**, *5*, 275.

(48) Bai, J.; Su, C. R.; Parra, R. D.; Zeng, X. C.; Tanaka, H.; Koga, K.; Li, J. M. *J. Chem. Phys.* **2003**, *118*, 3913.

(49) Kim, K. S.; Dupuis, M.; Kie, G. C.; Clementi, E. *Chem. Phys. Lett*. **1986**, *131*, 451.

(50) Dykstra, C. E. *J. Chem. Phys.* **1989**, *91*, 6472. Franken, K. A.; Jalaie, M.; Dykstra, C. E. *Chem. Phys. Lett.* **1992**, *198*, 59.

(51) Sabo, D.; Bacic, Z.; Bürgi, T.; Leutwyler, S. *Chem. Phys. Lett*. **1995**, *244*, 283.

(52) Tsai, C. J.; Jordan, K. D. *J. Chem. Phys.* **1991**, *95*, 3850.

(53) Tsai, C. J.; Jordan, K. D. *J. Phys. Chem.* **1993**, *97*, 5208.

(54) Lee, C.; Chen, H.; Fitzgerald, G. *J. Chem. Phys.* **1995**, *102*, 1266.

(55) Olthof, E. H. T.; van der Avoird, A.; Wormer, P. E. S. *J. Chem. Phys.* **1996**, *105*, 8034. Olthof, E. H. T.; van der Avoird, A.; Wormer, P. E. S.; Liu, K.; Saykally, R. J. *J. Chem. Phys.* **1996**, *105*, 8051.

(56) Gregory, J. K.; Clary, D. C. *J. Phys. Chem.* **1996**, *100*, 18014.

(57) Hartke, B.; Schutz, M.; Werner, H. J. *Chem. Phys*. **1998**, *239*, 561.

(58) Liu, K.; Cruzan, J. D.; Saykally, R. J. *Science* **1996**, *271*, 929 and references therein.

(59) Huisken, F.; Kaloudis, M.; Kulcke, A. *J. Chem. Phys.* **1996**, *104*, 17.

(60) Liu, K.; Brown, M. G.; Carter, C.; Saykally, R. J.; Gregory, J. K.; Clary, D. C. *Nature* **1996**, *381*, 501.

(61) Pribble, R. N.; Zwier, T. S. *Science* **1994**, *265*, 75.62.

(62) Watanabe, T.; Ebata, T.; Tanabe, S.; Mikami, N. *J. Chem. Phys.* **1996**, *105*, 408.

(63) Schmitt, M.; Jacoby, C.; Roth, W.; Kleinermanns, K. *J. Phys. Chem. A* **1998**, *102*, 4471.

(64) Gruenloh, C. J.; Carney, J. R.; Arrington, C. A.; Zwier, T. S.; Fredericks, S. Y.; Jordan, K. D. *Science* **1997**, *276*, 1678.

(65) Roth, W.; Schmitt, M.; Jacoby, C.; Spangenberg, D.; Janzen, C.; Kleinermanns, K. *Chem. Phys.* **1998**, *239*, 1.

(66) Buck, U.; Ettischer, I.; Melzer, M.; Buch, V.; Sadlej, J. *Phys. Rev. Lett.* **1998**, *80*, 2578.

(67) Brudermann, J.; Melzer, M.; Buck, U.; Kazimirski, J. K.; Sadlej, J.; Buch, V. *J. Chem. Phys.* **1999**, *110*, 10649.

(68) Sadlej, J.; Buch, V.; Kazimirski, J. K.; Buck, U. *J. Phys. Chem*. **1999**, *103*, 4933.

(69) Jorgensen, W. L.; Chandrasekhar, J.; Madura, J. D.; Impey, R. W.; Klein, M. L. *J. Chem. Phys.* **1983**, *79*, 926.

(70) Burnham, C. J.; Xantheas, S. S. *J. Chem. Phys.* **2002**, *116*, 5115.

(71) Torchet, G.; Schwartz, P.; de Feraudy, M. F.; Raoult, B. *J. Chem. Phys.* **1983**, *79*, 6196. Torchet, G.; Farges, J.; de Feraudy, M. F.; Raoult, B. *Ann. Phys. Fr.* **1989**, *14*, 245.

(72) Huang, J.; Bartell, L. S. *J. Phys. Chem.* **1994**, *98*, 7455. Huang, J.; Bartell, L. S. *J. Phys. Chem.* **1995**, *99*, 3924.

(73) (a) Devlin, J. P.; Joyce, C.; Buch, V. *J. Phys. Chem. A* **200**, *104*, 1974. (b) Devlin, J. P.; Buch, V. In *Water in Confining Geometries*; Buch, V., Devlin, P., Eds.; Springer: Berlin, 2003; Chapter 17.

(74) Delzeit, L.; Devlin, J. P.; Buch, V. *J. Chem. Phys.* **1997**, *107*, 3726.

(75) Buck, U.; Steinbach, C. In *Water in Confining Geometries*; Buch, V., Devlin, P., Eds.; Springer: Berlin, 2003; Chapter 3.

(76) Bauerecker, S. Private communication.

(77) Bauerecker, S.; Devlin, J. P.; Buck, U.; Kazimirski, J.; Buch, V. Invited paper for *Int. Rev. Phys. Chem*., in preparation.

(78) Hobbs, P. V. *Ice Physics*; Clarendon: Oxford, 1974.

(79) Petrenko, V. F.; Whitworth, R. W. *Physics of Ice*; Oxford University Press: New York, 1999.

(80) Buch, V.; Sandler, P.; Sadlej, J. *J. Phys. Chem. B* **1998**, *102*, 8641.

(81) Kuo, J. L.; Coe, J. V.; Singer, S. J.; Band, Y. B.; Ojamae, L. *J. Chem. Phys.* **2001**, *114*, 2527.

(82) Wawak, R. J.; Wimmer, M. M.; Scheraga, H. A. *J. Phys. Chem.* **1992**, *96*, 5138.

(83) Burnham, C. J.; Xantheas, S. S. *J. Chem. Phys.* **2002**, *116*, 1500.

(84) Wales, D. J.; Doye, J. P. K.; Miller, M. A.; Mortenson, P. N.; Walsh, T. R. *Adv. Chem. Phys.* **2000**, *115*, 1 and references therein.

(85) Matsumoto, M.; Saito, S.; Ohmine, I. *Nature* **2002**, *416*, 409.

(86) Berry, R. S. *J. Chem. Soc., Faraday Trans*. **1990**, *86*, 2343. Berry, R. S. *Theory of Atomic and Molecular Clusters*; Jellinek, J., Ed.; Springer: Berlin, 1999.

(87) Barkema, G. T.; de Boer, J. *J. Chem. Phys.* **1993**, *99*, 2059.

(88) Buch, V. *J. Chem. Phys.* **1992**, *97*, 726.

(89) Anderson, A. B. *J. Chem. Phys.* **1975**, *63*, 1499; **1976**, *65*, 4121.

(90) Li, Z.; Scheraga, H. A. *Proc. Natl. Acad. Sci. U.S.A.* **1987**, *84*, 6611.

(91) Ryckaert, J. P.; Ciccotti, G.; Berendsen, H. J. C. *J. Comput. Phys.* **1977**, *23*, 327.

(92) Zhang, Q.; Buch, V. *J. Chem. Phys.* **1990**, *92*, 5004.

(93) Tanaka, H.; Ohmine, I. *J. Chem. Phys.* **1989**, *91*, 6318.

(94) Suhm, M. A.; Watts, R. O. *Phys. Rep.* **1991**, *204*, 293.

(95) Kazimirski, J. K. In preparation.

(96) Stillinger, F. H. *Science* **1980**, *209*, 451.

(97) Visual inspection shows that the parent structure of 123A retained much of the crystallinity after initial surface relaxation (see section II.B). The crystallinity disappeared in the course of the MD+HNI optimization.

(98) The $n = 48$ sandwich structure was subjected to H-structure optimization to eliminate neighboring dangling H; we may not have found a lowest energy structure of this type, but significant additional energy gain due to H-bond optimization appears unlikely.